Control Performance Standards-Oriented Event-Triggered Load Frequency Control for Power Systems under Limited Communication Bandwidth

Xing-Chen Shangguan, *Graduate Student Member, IEEE*, Yong He, *Senior Member, IEEE*, Chuan-Ke Zhang, *Senior Member, IEEE*, Li Jin, *Graduate Student Member, IEEE*, Wei Yao, *Senior Member, IEEE*, Lin Jiang, *Member, IEEE* and Min Wu, *Fellow, IEEE*

***Abstract*—Load frequency control (LFC) of modern power systems tends to employ open communication networks to transmit measurement/control signals. Under a limited network bandwidth, the continuous and high-sampling-rate signal transmission will be prone to degradation of the LFC performance through network congestion. This paper proposes a decentralized control performance standards (CPSs)-oriented event-triggered LFC scheme for power systems under constrained communication bandwidth. The proposed scheme comprises the event-triggered LFC scheme and the CPSs-oriented regulation scheme. In the CPSs-oriented regulation scheme, regulation rules are designed to adjust the threshold parameter of the event-triggered LFC scheme based on the North American Electrical Reliability Council (NERC)'s CPS1 and CPS2. The rules generate a larger threshold parameter to lower the triggering frequency in order to reduce unnecessary transmission of measurement/control signals, while ensuring the frequency and tie-lie power of the power systems to meet the required CPS1 and CPS2 instead of the asymptotic stability requirement in the existing research. The reduced transmission of these signals lessens the communication burden. In addition, the decentralized control strategy is used to solve the problems of poor large scalability and computational dimension caused by the centralized control strategy. The effectiveness of the proposed scheme is evaluated on an IEEE 39-bus test system with renewable energy sources.**

***Index Terms*—Power systems, Load frequency control, Open communication network, NERC's CPS1 and CPS2, Event-triggered control.**

NOMENCLATURE

LFC	Load frequency control
NERC	North American Electrical Reliability Council
CPS1/2	Control performance standard 1/2
TT	Time-triggered
ET, AET	Event-triggered, adaptive event-triggered
CPSO	Control performance standards oriented
ACE	Area control error
EDR	Exponential decay rate
LMI	Linear matrix inequality
TAMC	Transmission amount of measurement/control signals
NAL	Numbers of $\|(ACE_i)_{10min}\| \leq L_{10-i}$
Δf_i	Frequency deviation
ΔP_{vi}	Valve position deviation
ΔP_{mi}	Generator mechanical output deviation
ΔP_{di}	Load change
ΔP_{tie-i}	Net tie-line power flow deviation
β_i	Frequency bias factor
R_i	Speed drop
M_i	Moments of inertia of the generator
D_i	Damping coefficient of the generator
T_{chi} & T_{gi}	Time constant of turbine and governor
T_{ij}	Tie-line synchronizing coefficient between area i and area j

This work was supported in part by the National Natural Science Foundation of China under Grants 62022074, 61973284 and 61873347, by the Hubei Provincial Natural Science Foundation of China under Grants 2019CFA040, by the 111 project under Grant B17040, by the National Key R&D Program of China under Grant 2017YFB1300900, and by the Fundamental Research Funds for National Universities, China University of Geosciences (Wuhan). *(Corresponding author: Chuan-Ke Zhang)*

X.C. Shangguan, Y. He, C.K. Zhang, L. Jin, and M. Wu are with the School of Automation, China University of Geosciences, Wuhan 430074, China, with the Hubei Key Laboratory of Advanced Control and Intelligent Automation for Complex Systems, Wuhan 430074, China, and also with the Engineering Research Center of Intelligent Technology for Geo-Exploration, Ministry of Education, Wuhan 430074, China. (email: star@cug.edu.cn; heyong08@cug.edu.cn;ckzhang@cug.edu.cn;jinli@cug.edu.cn;wumin@cug.edu.cn).

W. Yao is with the State Key Laboratory of Advanced Electromagnetic Engineering and Technology, Huazhong University of Science and Technology, Wuhan 430074, China.(email: w.yao@hust.edu.cn).

L. Jiang is with the Department of Electrical Engineering and Electronics, University of Liverpool, Liverpool L69 3GJ, United Kingdom.(email: Ljiang@liv.ac.uk).

I. INTRODUCTION

The main objective of load frequency control (LFC) is to balance the load and the generation in order to maintain frequency and tie-line power with neighborhood areas at scheduled values [1], [2]. The traditional LFC scheme employs a dedicated communication channel to transmit measurement/control signals. However, it is noted in [3] that an effective modern power system tends to use an open communication network to support the increasingly decentralized property of control services due to the introduction of renewable energy sources and the increased interaction with the demand-side response. Although an open communication network can provide many advantages such as low cost and flexibility, its introduction presents new challenges, including transmission delays, packet losses and parametric uncertainties [4].

Much attention has been paid to the analysis/synthesis of LFC with transmission delays, packet losses and parametric uncertainties. For example, Yu et al. [5] developed a full state-feedback robust LFC scheme that can ensure good performance despite indeterminate delays in the communication network. Jiang et al. carried out a series of work to investigate the delay-dependent stability and obtain the time delay margin for the PID-type LFC scheme [6]–[8]. Zhang et al. [9] proposed a delay-dependent PID-type robust LFC scheme for time-delay power systems, while Trip et al. [10] introduced a passivity-based optimal LFC scheme to handle

the parametric uncertainties based on slide-mode control. Considering the sampling characteristic in practical LFC, Luo et al. [11] explored the stability problem of LFC with both sampling and transmission delays, while a robust PI-type LFC scheme was proposed in [12]. Additionally, a switching system-based approach was introduced to the LFC scheme that is resilient to DoS attacks [13]. However, in an open communication network with limited bandwidth, heavy usage of bandwidth will aggravate the problems of transmission delays, packet losses and parametric uncertainties. At this time, the existing robust LFC schemes may not be effective. Note that the practical communication network among generation units faces the bandwidth constraint [14]. Additionally, the LFC scheme may be embedded with microprocessors, which usually run with limited computing capability and energy resources [15]. Therefore, for modern power systems with heavy transmission burdens, it would be desirable to design an effective LFC scheme to reduce the communication and computational burdens.

Recent literature reveals that there are two main methods to reduce the transmission amounts of measurement/control signals in communication networks. One way is to maximize the sampling interval based on a time-triggered sampled-data control scheme. Dahiya et al. [16] developed a larger sampling interval for isolated hybrid power system, while a maximal acceptable sampling interval was obtained for multi-area power systems in [17]. Another way is to change the trigger mechanism of data transmission. Wen et al. [15], [18] introduced an event-triggered (ET) communication scheme to alleviate communication burdens for multi-area power systems, where the periodically sampled data are only transmitted when a preset threshold condition is violated. As an improvement, Dong et al. [19] proposed an ET control architecture for LFC of multi-area power systems with supplementary adaptive dynamic programming, while Liu et al. [20] proposed an LFC scheme with the co-design of ET communication scheme and distributed model-based controller. In addition, Peng et al. [21] developed an adaptive event-triggered (AET) control scheme, where the threshold parameter in the AET control scheme can be adaptively adjusted to conserve more limited network resources. Similar to [21], Li et al. [22] proposed an AET-based sliding mode LFC for a multi-area interconnected microgrid power systems, while Zhang e al. designed an AET LFC scheme for multi-area uncertain power systems in [23].

The above control schemes, however, all focus on the asymptotic stability for power system frequency and tie-lie power. In fact, based on the North American Electrical Reliability Council (NERC), the frequency and tie-lie power only need to comply with control performance standard 1 (CPS1) and CPS2 [24]. The standards require frequency and tie-lie power to fluctuate within a certain range, rather than asymptotic stability, which undoubtedly relaxes the requirements of LFC design. The standards have been applied by several scholars to guide the design of LFC to reduce the wear and tear of the generating units. For example, Feliachi et al. presented a CPS-compliant fuzzy logic rules-based LFC scheme [25], [26], while Pappachen et al. introduced a control performance standards oriented (CPSO) adaptive neuro-fuzzy interface system controller for LFC of multi-area deregulated power systems [27]. However, these research endeavors considered neither the event-triggered communication scheme nor the transmission delay and sampling characteristics in the open communication network environment. In addition, most of the above control schemes (excluding [18]) are based on centralized control strategies, where the processing and communication infrastructure require limited scalability of the multi-area power system, as noted in [4]. Moreover, the system dimensions significantly increase with added control area. To overcome these problems of the centralized LFC scheme, the decentralized LFC scheme has been developed. Such a scheme, which reduces the computational burden of passage of the communication between different systems and makes the control more feasible and simple, has been widely used in LFC as reported in [28] and [29]. Therefore, it is desirable to design a decentralized LFC scheme with the aid of the CPSs to further reduce signal transmission.

Motivated by the above discussions, this paper develops a CPSO-ET LFC scheme for power systems under limited communication bandwidth. The main contributions of this paper are as follows.

1) The proposed CPSO-ET LFC scheme consists of two parts: the ET LFC scheme and the CPSO regulation scheme. In the CPSO regulation scheme, the regulation rules based on CPS1 and CPS2 are designed to adjust the threshold parameter of the ET scheme.
2) CPS1 and CPS2 are used as the aim of the regulation rules rather than the asymptotic stability condition, which relaxes the constraints of the threshold parameter selection compared with the previous research in [15] and [21] and ensures that the power system frequency and tie-lie power meet the required CPS1 and CPS2.
3) The selection of a large threshold parameter in the ET scheme lowers the triggering frequency to further reduce the unnecessary transmission of measurement/control signals. This approach significantly alleviates communication burden.
4) The decentralized control strategy is applied for the distributed power system in this paper instead of the centralized control strategy used in [15] and [21], which reduces the computational complexity and improves the scalability of the system.

The remainder of this paper is organized as follows. Section II presents the decentralized ET LFC model. Section III describes the design procedure of the proposed CPSO-ET LFC scheme. In Section IV, case studies based on the IEEE 39-bus test system are shown to verify the effectiveness of the proposed scheme. The conclusion is presented in Section V.

II. Modeling for Decentralized ET LFC

In this section, a decentralized ET LFC model of a multi-area power system is constructed.

A. Decentralized LFC Model with Communication Networks

The linearized LFC transfer function model of control area i of an N-area power system is demonstrated in Fig. 1, which includes governor, turbine, rotating mass and load, tie-line power, and communication channel, where v_i =

$\sum_{j=1,j\neq i}^{n} T_{ij}\Delta f_j$; ACE_i represents the area control error (ACE) of the i_{th} area of the power system and is the linear combination of Δf_i and ΔP_{tie-i}, i.e., $ACE_i = \beta_i \Delta f_i + \Delta P_{tie-i}$. Assume that the generator is equipped with a non-reheat turbine.

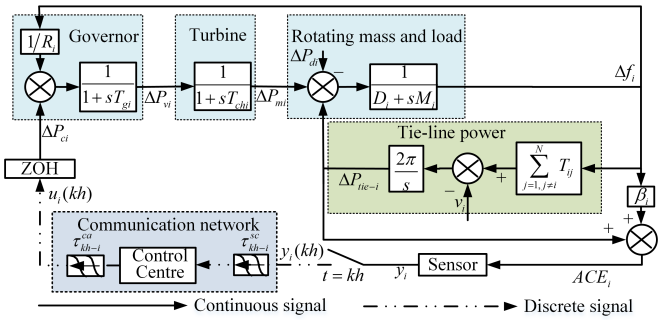

Fig. 1. LFC structure of control area i of N-area power systems

The decentralized control strategy is applied to the multi-area LFC scheme. The interactions between different areas, i.e., v_i, are treated as disturbances for every area. This means that every control area is independent and has its own LFC center to maintain the balance of generation and load. We then represent the LFC scheme of area i as the following state space model [1]:

$$\begin{cases} \dot{\bar{x}}_i(t) = \bar{A}_i\bar{x}_i(t) + \bar{B}_i u_i(t) + \bar{F}_i\omega_i(t) \\ \bar{y}_i(t) = \bar{C}_i\bar{x}_i(t) \end{cases} \tag{1}$$

where

$\bar{x}_i^T = [\Delta f_i\ \Delta P_{tie-i}\ \Delta P_{mi}\ P_{vi}],\ u_i = \Delta P_{ci},\ \bar{y}_i = ACE_i$

$\omega_i = [\Delta P_{di}\ v_i]^T,\ \bar{B}_i = [0\ 0\ 0\ \frac{1}{T_{gi}}]^T,\ \bar{C}_i = [\beta_i\ 1\ 0\ 0]$

$$\bar{A}_i = \begin{bmatrix} -\frac{D_i}{M_i} & -\frac{1}{M_i} & \frac{1}{M_i} & 0 \\ 2\pi\sum_{j=1,j\neq i}^{N} T_{ij} & 0 & 0 & 0 \\ 0 & 0 & -\frac{1}{T_{chi}} & \frac{1}{T_{chi}} \\ -\frac{1}{R_{1i}T_{gi}} & 0 & 0 & -\frac{1}{T_{gi}} \end{bmatrix} \bar{F}_i = \begin{bmatrix} -\frac{1}{M_i} & 0 \\ 0 & -2\pi \\ 0 & 0 \\ 0 & 0 \end{bmatrix}.$$

If there are n generators, which are all responsible for the secondary frequency control task, then the control input ΔP_{ci} will be assigned to every generator according to participation factor α_{ki}. The multi-generator LFC model of every control area can be found in Ref. [9].

The following PI-type controller is chosen

$$\begin{cases} \bar{y}_i(t) = ACE_i(t) \\ u_i(t) = -K_{Pi}\bar{y}_i(t) - K_{Ii}\int \bar{y}_i(t) \end{cases} \tag{2}$$

where K_{Pi} and K_{Ii} are the proportional gain and integral gain, respectively. Note that the output signal $\bar{y}_i(t)$ cannot be directly used due to the characteristic of periodic sampling and the communication delay in the communication network. The attainable $\bar{y}_i(t)$ can be written as follows.

$$\bar{y}_i(t) = \bar{y}_i(kh), t \in [kh + \tau_{kh,i}, (k+1)h + \tau_{(k+1)h,i}) \tag{3}$$

where $k = 0, 1, 2, \cdots$, $\tau_{kh,i} = \tau_{kh,i}^{sc} + \tau_{kh,i}^{ca} \leq \tau_M$; $\tau_{kh,i}$ is the sum of the network-induced delays $\tau_{kh,i}^{sc}$ (from sensor to controller) and $\tau_{kh,i}^{ca}$ (from controller to actuator); τ_M is the known maximum sum of the delays; and h is the sampling period. By combining (2) with (3), for $t \in [kh + \tau_{kh,i}, (k+1)h + \tau_{(k+1)h,i})$, the PI controller is designed as

$$u_i(t) = u_i(kh) = -K_{Pi}\bar{y}_i(kh) - K_{Ii}\int \bar{y}_i(kh) \tag{4}$$

Defining $x_i(t) = [\bar{x}_i^T(t)\ \int \bar{y}_i^T(t)]^T$ and $y_i(t) = [\bar{y}_i^T(t)\ \int \bar{y}_i^T(t)]^T$ and substituting (4) into (1), the closed-loop LFC model of area i can be formalized as

$$\begin{cases} \dot{x}_i(t) = A_i x_i(t) - B_i K_i C_i x_i(kh) + F_i\omega_i(t) \\ y_i(t) = C_i x_i(t), t \in [kh + \tau_{kh,i}, (k+1)h + \tau_{(k+1)h,i}) \end{cases} \tag{5}$$

where $k = 0, 1, 2, \cdots$, $K_i = [K_{Pi}\ K_{Ii}]$ and

$$A_i = \begin{bmatrix} \bar{A}_i & 0 \\ \bar{C}_i & 0 \end{bmatrix}, B_i = \begin{bmatrix} \bar{B}_i \\ 0 \end{bmatrix}, C_i = \begin{bmatrix} \bar{C}_i & 0 \\ 0 & 1 \end{bmatrix}, F_i = \begin{bmatrix} \bar{F}_i \\ 0 \end{bmatrix}.$$

B. ET LFC Scheme

The following ET algorithm [21] is applied in LFC to decide the future transmitted sampling instant $t_{k+1}h$.

$$\begin{cases} t_{k+1}h = t_k h + \min_{j\in\mathbb{N}}\{jh | \partial_1(jh)\} \\ \partial_1(jh): y_e^T(ijh)\varpi_i y_e(ijh) - \delta_i y_i^T(t_k h)\varpi_i y_i(t_k h) > 0 \end{cases} \tag{6}$$

where δ_i is the threshold parameter; ϖ_i is a positive definite weighting matrix; and $y_e(ijh) = y_i(ijh) - y_i(t_k h)$, $ijh = t_k h + jh$, $j \in \mathbb{N}$, $t_k (k = 0, 1, 2, \ldots)$ are some integers such that $\{t_0, t_1, t_2, \ldots\} \subset \{0, 1, 2, \ldots\}$. Based on (5), $y_i(t) = C_i x_i(t)$, so condition (6) can be rewritten as

$$\begin{cases} t_{k+1}h = t_k h + \min_{j\in\mathbb{N}}\{jh | \partial_2(jh)\} \\ \partial_2(jh): e^T(ijh)\Omega e(ijh) - \delta_i x_i^T(t_k h)\Omega x_i(t_k h) > 0 \end{cases} \tag{7}$$

where $\Omega = C_i^T\varpi_i C_i$; $e(ijh) = x_i(ijh) - x_i(t_k h)$. Under this scheme, the sampling data in (3) cannot be transmitted over the communication networks unless condition (7) is satisfied. Then, the PI control law can be written as

$$u_i(t) = u_i(t_k h) = -K_i y_i(t_k h) = -K_i C_i x_i(t_k h),\ t \in \Pi \tag{8}$$

where $\Pi = [t_k h + \tau_{t_k h,i}, t_{(k+1)}h + \tau_{t_{(k+1)}h,i})$. The interval Π is divided into the following subsets Π_j

$$\Pi = \bigcup \Pi_j,\ \ \Pi_j = [i_j h + \tau_{t_k}, i_j h + h + \tau_{t_{k+j}}]$$

where $i_j = t_k + j$, $j = 0, 1, \ldots, t_{k+1} - t_k - 1$, and

$$\tau_{t_k+j} = \begin{cases} \tau_{t_k}, j = 0, 1, \ldots, t_{k+1} - t_k - 2 \\ \tau_{t_{k+1}}, j = t_{k+1} - t_k - 1 \end{cases}$$

Define $\varsigma(t) = t - i_j h$, $t \in \Pi_j$. It is clear that $\varsigma(t)$ is a piecewise-linear function satisfying $\dot{\varsigma}(t) = 1$, $\tau_{t_k} \leq \varsigma(t) \leq h + \tau_{t_{k+j}} \leq \bar{\varsigma} = h + \tau_M$ when $t \neq i_j h + \tau_{t_k}$. Additionally, the control law (8) can be rewritten as

$$u_i(t) = u_i(t_k h) = K_i C_i(e(i_j h) - x_i(t - \varsigma(t))),\ t \in \Pi_j \tag{9}$$

By replacing (4) with (9), the ET LFC model of area i can be formulated as

$$\begin{cases} \dot{x}_i(t) = A_i x_i(t) + B_i K_i C_i(e(i_j h) - x_i(t - \varsigma(t))) + F_i\omega(t) \\ y_i(t) = C_i x(t),\ \ t \in \Pi_j \end{cases} \tag{10}$$

The initial condition of $x(t)$ on $[\tau_{t_0} - \bar{\varsigma}, \tau_{t_0}]$ is supplemented as $x(t) = \varphi(t)$, $t \in [\tau_{t_0} - \bar{\varsigma}, \tau_{t_0}]$, with $\varphi(\tau_{t_0}) = x(\tau_{t_0}) = x_0$, where $\varphi(t)$ is a continuous function [31].

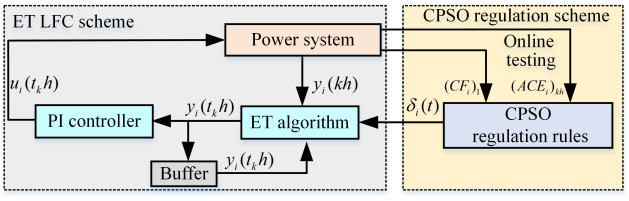

Fig. 2. CPSO-ET LFC scheme

III. Design of CPSO-ET LFC Scheme

The proposed scheme comprises two parts, as shown in Fig. 2. One is the ET LFC scheme, which determines the next triggering time $t_{k+1}h$ by analyzing $\delta_i(t)$, $y_i(kh)$ and $y_i(t_k h)$. $\delta_i(t)$ is the threshold parameter of the ET algorithm; $y_i(kh)$ represents the periodically sampled data of $y_i(t)$; and $y_i(t_k h)$ represents the latest updated data of $y_i(t)$. The other part is the CPSO regulation scheme, which adjusts the threshold

parameter $\delta_i(t)$ based on online evaluations of CPS1 and CPS2. To complete the design of the proposed scheme, the basic thing is to develop gains of PI controller, initial threshold parameter and weighting matrix to ensure the stability of the ET LFC scheme. Then, based on the stable ET LFC schemes, the threshold parameter is adjusted by evaluating CPS1 and CPS2 rather than the stability of the whole system.

A. Design of ET LFC scheme

Motivated by the fast LFC design in [17], the exponential stabilization condition of the ET LFC scheme is derived to obtain the gains of the PI controller with a certain dynamical performance.

Theorem 1: Consider system (10) with $\omega(t)=0$. For given sampling period h, transmission delay τ_M, exponential decay rate (EDR) λ, threshold parameter δ and tuning parameters a and b, system (10) is exponentially stable with an EDR λ if there are symmetric matrices $(\hat{P}_2)_{2r\times 2r}$, $(\hat{Z})_{r\times r}$ and $(\hat{X})_{2r\times 2r}=\begin{bmatrix}\hat{X}_1+\hat{X}_1^T & -\hat{X}_1-\hat{X}_2\\ * & \hat{X}_2+\hat{X}_2^T\end{bmatrix}$, and symmetric positive definite matrices $(\hat{P}_1)_{2r\times 2r}$, $(\hat{P}_3)_{r\times r}$, $(\hat{\Omega})_{r\times r}$ and any appropriately dimensioned matrices $\hat{S}$, $\hat{M}$ and $Y=K_iC_i\hat{S}^T$, for $f=1,2$ such that the following linear matrix inequalities (LMIs) hold

$$\hat{\Xi}_{1f}=\hat{\psi}_1+\hat{\Gamma}_f+h\hat{\psi}_2<0 \tag{11}$$

$$\hat{\Xi}_{2f}=\begin{bmatrix}\hat{\psi}_1+\hat{\Gamma}_f & -h\hat{\Upsilon}_2^T\hat{M}\\ * & -h\hat{Z}\end{bmatrix}<0 \tag{12}$$

where

$$\begin{aligned}\hat{\psi}_1=&Sym\left\{\begin{bmatrix}e_1\\e_3\end{bmatrix}^T\hat{P}_1\begin{bmatrix}e_5\\e_4\end{bmatrix}+\Upsilon_2^T\hat{M}(e_1-e_2)\right\}-\begin{bmatrix}e_3\\e_2\end{bmatrix}^T\hat{X}\begin{bmatrix}e_3\\e_2\end{bmatrix}\\&+\begin{bmatrix}e_1\\e_5\end{bmatrix}^T\hat{P}_2\begin{bmatrix}e_1\\e_5\end{bmatrix}-\begin{bmatrix}e_3\\e_4\end{bmatrix}^T\hat{P}_2\begin{bmatrix}e_3\\e_4\end{bmatrix}+\tau_Me_5^T\hat{P}_3e_5\\&-\tfrac{1}{\tau_M}(e_1-e_3)^T\hat{P}_3(e_1-e_3)+\delta e_2^T\hat{\Omega}e_2-e_6^T\hat{\Omega}e_6\\\hat{\Gamma}_f=&Sym\{\hat{\Upsilon}_1^T\hat{\Upsilon}_3(e_5-(A_i+\lambda I)e_1-\rho_fB_iY(e_6-e_2))\}\\\hat{\psi}_2=&e_4^T\hat{Z}e_4+Sym\left\{\begin{bmatrix}e_3\\e_2\end{bmatrix}^T\hat{X}\begin{bmatrix}e_4\\0_{r\times 6r}\end{bmatrix}\right\},\rho_1=e^{\lambda\tau_M},\rho_2=e^{\lambda\eta_M}\\e_l=&\begin{bmatrix}0_{r\times(l-1)r}I_r0_{r\times(6-l)r}\end{bmatrix},l=1,\cdots,6,\hat{\Upsilon}_3=[I_r;aI_r;bI_r]\\\hat{\Upsilon}_1=&\begin{bmatrix}e_1^T&(e_6-e_2)^T&e_5^T\end{bmatrix}^T,\ \hat{\Upsilon}_2=\begin{bmatrix}e_1^T\cdots e_6^T\end{bmatrix}^T\end{aligned}$$

and r is the dimension of matrix A_i in system (10); I and 0 represent the identity matrix and a zero matrix, respectively; the superscript T represents the transpose, the superscript -1 represents the inverse, and $diag\{\cdots\}$ stands for a block-diagonal matrix; the notation $*$ always denotes the symmetric block in a symmetric matrix; for any square matrix $\mathbb{A}$, we define $Sym\{\mathbb{A}\}=\mathbb{A}+\mathbb{A}^T$; and if the dimensions of matrices are not explicitly stated, they are assumed to have compatible dimensions for algebraic operations.

Moreover, controller gains K_i can be calculated by

$$K_i=Y(\hat{S}^T)^{-1}C_i^T(C_iC_i^T)^{-1}. \tag{13}$$

The proof is shown in Appendix A.

Note that the margin δ_M of the threshold parameter that ensures the stability of the ET LFC scheme can be obtained by Steps 1 and 2 in following Algorithm 1. Then, the initial threshold $\delta_i(0)$ in the following CPSO regulation scheme belongs to $(0,\delta_M]$.

B. Design of the CPSO regulation scheme

We first revisit the concepts of CPS1 and CPS2 in NERC [24]. CPS1 assesses the impact of ACE on frequency over 12-month window or horizon and it is expressed as

$$CPS1_i=(2-CF_i)\times 100\% \tag{14}$$

where $CF_i=AVG_{12-month}[(CF_i)_1]$ is a compliance factor of area i and

$$(CF_i)_1=\left[\left(\frac{ACE_i}{-10\beta_i}\right)_1\left(\frac{\Delta f_i}{\varepsilon_1^2}\right)_1\right] \tag{15}$$

where ε_1 represents the targeted frequency bound for CPS1 and $(\cdot)_1$ is the clock-1-min average. To comply with NERC, CPS1 should not be less than 100%. CPS2 requires the 10-min averages of a control area's ACE to be less than a constant (L_{10-i}) given in the equation below.

$$(ACE_i)_{10min}\le L_{10-i}=1.65\varepsilon_{10}\sqrt{(-10\beta_i)(-10\beta_s)} \tag{16}$$

where$(ACE_i)_{10min}$ is the 10-min average of the area's ACE, β_s is the summation of the frequency bias of all control areas in the considered interconnection, and ε_{10} is the targeted frequency bound for CPS2. To comply with this standard, each control area needs to have its compliance no less than 90%. A compliance percentage is calculated by the following equation

$$CPS2_i=100\left(1-\frac{Num((ACE_i)_{10min}>L_{10-i})}{Num(all|(ACE_i)_{10min})}\right)\% \tag{17}$$

where $Num((ACE_i)_{10min}>L_{10-i})$ denotes the number of $(ACE_i)_{10min}$ that satisfies $(ACE_i)_{10min}>L_{10-i}$ in one month, and $Num(all|(ACE_i)_{10min})$ represents the number of all $(ACE_i)_{10min}$ in one month.

As shown in event-triggered condition (7), the triggering frequency depends on the threshold parameter. The larger the threshold parameter, the more difficult it is to trigger, which reduces more unnecessary signal transmission. Now, we are in a position to introduce the CPSO regulation scheme to adjust the threshold parameter.

The power system frequency and ACE are measured periodically and then averaged statistically to evaluate CPS1 and CPS2 based on their definitions. The objective of CPS1 is to ensure that the average CF_i of 1-minute average $(CF_i)_1$ during a 12-month period is not higher than 1, while the objective of CPS2 is to ensure that the 10-minute average of ACE is less than L_{10-i}. It is obvious that if $(CF_i)_1\le 1$ and the ACE of every sampling time $(ACE_i)_{kh}\le L_{10-i}$, then the objectives of CPS1 and CPS2 can be achieved, respectively. Therefore, the $(CF_i)_1$ and $(ACE)_{kh}$ are measured and are compared with the given constants 1 and L_{10-i}, respectively, to design the following regulation rules. The rules are divided into two parts. The first part is based on the measurements of $(ACE)_{kh}$ of CPS2.

$$\Theta_i(kh)=\begin{cases}\delta_i((k-1)h)+\dfrac{2\delta_i(0)}{\pi}\text{atan}\left(\dfrac{10\Phi_i}{\delta_i(0)}\right),\Phi_i>0\\ \delta_i((k-1)h)\left(1+\dfrac{2}{\pi}\text{atan}\left(\delta_i(0)\Phi_i\right)\right),\Phi_i\le 0\end{cases} \tag{18}$$

where $\delta_i(0)$ is the initial preset threshold parameter; $\Phi_i=L_{10-i}-(ACE_i)_{kh}$. By comparing $(ACE_i)_{kh}$ and L_{10-i} at every sampling instant, if $\Phi_i\le 0$, $\Theta_i(kh)$ will be reduced to $1+\frac{2}{\pi}\text{atan}\left(\delta_i(0)\Phi_i\right)$ times the threshold parameter $\delta_i((k-1)h)$ at the previous sampling instant $(k-1)h$; if $\Phi_i>0$, $\Theta_i(kh)$ will increase by $\frac{2\delta_i(0)}{\pi}\text{atan}\left(\frac{10\Phi_i}{\delta_i(0)}\right)$.

Then, the second part is based on the measurements of $(CF_i)_1$ of CPS1.

$$\delta_i(kh)=\min\{\bar{\delta}_i,\eta_i(kh)\Theta_i(kh)\} \tag{19}$$

where

$$\eta_i(kh) = \begin{cases} 1, (CF_i)_1 < 1 \\ 1 - \dfrac{2\alpha}{\pi} \text{atan}\left[(CF_i)_1 - 1\right], (CF_i)_1 \geq 1 \end{cases} \tag{20}$$

and α is the controllable parameter with $0 < \alpha \leq 1$, and $\bar{\delta}_i$ is the preset maximum of $\delta_i(t)$. If $(CF_i)_1 \geq 1$, then $\eta_i(kh) < 1$ and $\delta_i(kh)$ will decrease; if $(CF_i)_1 < 1$, then $\eta_i(kh) = 1$ and $\delta_i(kh)$ will be equal to the minimum between $\bar{\delta}_i$ and $\Theta_i(kh)$.

Remark 1: The rules are determined artificially based on the $atan$ function and the input of online measurements $(CF_i)_1$ and $(ACE_i)_{kh}$. This is similar to the *reward and punishment* mechanism to regulate threshold parameter based on the difference between the measurements and the required values. Note that the function $atan(\cdot)$ has the lower and upper bounds: that is, $atan(\cdot) \in (-\pi/2, \pi/2)$. This property is effectively used in equation (18) to adjust the event-triggered threshold parameter [21]. Additionally, $\delta_i(0)$ is used here to regulate the sensitivity of the rule: that is, the smaller $\delta_i(0)$ is, the lower the sensitivity is.

Remark 2: In the AET LFC scheme [21]–[23], the regulation rules are derived to regulate the threshold parameter based on system output $y_i(kh)$, which is still limited to the asymptotic stability of frequency and ACE. In this paper, CPS1 and CPS2 are used to guide the regulation rules, which guarantees CPS1 and CPS2 of the power system and relaxes the constraint of the selection of threshold parameters.

Remark 3: Note that the values of $(CF_i)_1$ do not rapidly decrease immediately when disturbances or system faults occur. Due to the inherent characteristic of large inertia in LFC, the changes in frequency and the tie-line power of the system are slow. Additionally, $(CF_i)_1$ is the 1-minute average of the measurements of the frequency and tie-line power. Within one minute, the abnormal changes in the frequency and tie-line power in a short time can be compensated by other normal values.

C. CPSO-ET LFC scheme

In this subsection, we introduce the following Algorithm 1 to explain the detailed design procedure of the proposed scheme to obtain the necessary transmission instant $t_k h$ based on the ET LFC scheme and CPSO regulation scheme.

Algorithm 1: Obtain the transmission instant $t_k h$.

Step 1 Preset initial parameters: A_i, B_i, C_i, τ_M, h and λ.

Step 2 Find $\delta_i(0)$, K_i and ϖ_i.

1) Initialize the search interval $[\delta_{min}, \delta_{max}]$ with $\delta_{min} = 0$ and large enough number δ_{max} and select the accuracy coefficient $\delta_{ac} = 0.0001$.
2) Check the feasibility of LMIs (11) and (12) under $\delta_{test} = (\delta_{min} + \delta_{max})/2$. If (11) and (12) are feasible, set $\delta_{min} = \delta_{test}$; else, set $\delta_{max} = \delta_{test}$.
3) If $|\delta_{min} - \delta_{max}| \leq \delta_{ac}$, obtain the maximal $\delta_M = \delta_{min}$. If $\delta_M > 0$, then obtain $\delta_i(0) = \delta_M$ and go to 4); else, no feasible $\delta_i(0)$.
4) Obtain matrices $\hat{S}$, Y and Ω from LMIs (11) and (12). Calculate K_i and ϖ_i from equation (13) and $\varpi_i = (C_i C_i^T)^{-1} C_i \Omega C_i^T (C_i C_i^T)^{-1}$, respectively.

Step 3 Set the defaults: h, τ_M, K_i, $\delta_i(0)$, ϖ_i, $\bar{\delta}$, α, $y_i(t_0 h) = 0$, the stored transmission signal $y_i(sh) = y_i(t_0 h)$, and $k = j = 1$.

Step 4 Monitor and store $ACE_i(jh)$, $\Delta f_i(jh)$. Then, derive $y_i(jh)$. Calculate Φ_i and obtain $\Theta_i(jh)$ based on equation (18). Then, calculate $\eta_i(jh)$ and derive $\delta_i(jh)$ based on equations (19) and (20).

Step 5 Based on the current $y_i(jh)$ and the stored transmission signal $y_i(sh)$, calculate the value of $y_e(jh)$, $y_e(jh) = y_i(jh) - y_i(sh)$ and find the transmission instant $t_k h$.

1) Based on the values of ϖ_i, $\delta_i(jh)$ and $y_e(jh)$ and the ET condition (6), obtain inequality $\partial_1(jh)$.
2) If inequality $\partial_1(jh)$ is satisfied, output and store transmission signal $y_i(jh)$, and take $t_k h$ as the transmission instant, and $t_k = j$. Then, update the stored transmission signal $y_i(sh) = y_i(t_k h)$, and set $k = k+1$ and $j = j+1$. If not, set $j = j + 1$. Repeat Steps 4 and 5.

Remark 4: The PI controller gains and initial threshold parameters obtained by Theorem 1 ensure the stability of the ET LFC system when the CPSO regulation scheme is not used. When the regulation scheme is used, it adjusts the threshold parameters in ET LFC based on the online measurements of CPS1 and CPS2 to influence whether the measurement/control signals are updated and does not change the PI controller gains. The regulation scheme ensures the power system frequency and tie-line power to fluctuating within an acceptable range to meet CPS1 and CPS2 of NERC, which guarantees that the output of the system is bounded.

Remark 5: Compared with ET LFC based on the centralized control strategy in [21]–[23], the proposed scheme based on the decentralized control strategy ensures scalability in large-scale interconnected power systems. The power systems are divided into different control areas. The corresponding control and communication parameters in the proposed scheme can be obtained by Algorithm 1 for different control areas. In the CPSO regulation scheme, the controller gains are constant and only the threshold parameters are regulated.

IV. Case Studies

In this section, case studies are carried out based on an IEEE 39-bus test system to illustrate the superiority of the proposed LFC scheme in reducing the communication burden, as well as the effectiveness of ensuring that the system frequency and ACE satisfy the CPSs of NERC.

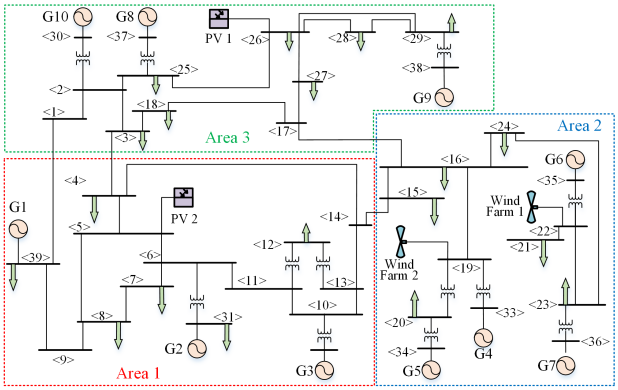

Fig. 3. Single-line diagram of IEEE 39-bus test system.

A. IEEE 39-Bus Test System

The IEEE 39-bus test system is shown in Fig. 3. The test system is modified by adding four sections of renewable energy sources, i.e. two photovoltaic (PV) power stations in buses 5 and 26, and two wind farms in buses 19 and 22. This system consists of 10 generators, 19 loads, 34 transmission lines, and 12 transformers. The generators are equipped with excitation and power system stabilizer units. The power system is divided into three control areas. Assume that every generator in each area is responsible for the secondary frequency regulation

task. The simulation parameters for the generators, loads, lines and transformers are given in [34]; the parameters of wind turbine and PV are given in 24-hour simulation of a Vehicle-to-Grid System in MATLAB(2015a); and the parameters of the governor, the turbine and the participation factor of every generator are shown in Table I. The generation rate constraints for every generator are considered to be ± 0.1 pu/min.

TABLE I
PARAMETERS OF GOVERNOR, TURBINE AND PARTICIPATION FACTOR

Area 1	α_{11}=0.2, α_{21}=α_{31}=0.4, T_{ch1}=0.3, T_{g1}=0.1
Area 2	α_{12}=α_{42}=0.2, α_{22}=α_{32}=0.3, T_{ch2}=0.35, T_{g2}=0.17
Area 3	α_{13}=α_{23}=0.2, α_{33}=0.6, T_{ch3}=0.4, T_{g3}=0.2

B. Implementation of The CPSO-ET Scheme

Assume sampling period and the maximal acceptable transmission delay are 4s and 1s , respectively, in each control area of the power system. The EDRs are set to 0.1, 0.08 and 0.1 in areas 1, 2 and 3, respectively. Then we obtain the following parameters based on Algorithm 1:

	$\delta_i(0)$	K_i	ϖ_i
Area 1	0.0235	-[0.2257 0.1197]	$\begin{bmatrix} 0.0626 & -124.50 \\ -124.50 & 9.10e+05 \end{bmatrix}$
Area 2	0.0235	-[0.0380 0.1793]	$\begin{bmatrix} 1.0950 & -1396.30 \\ -1396.30 & 2.97e+06 \end{bmatrix}$
Area 3	0.0235	-[0.0401 0.1196]	$\begin{bmatrix} 0.2156 & -153.10 \\ -153.10 & 2.10e+05 \end{bmatrix}$

These parameters are applied to the CPSO-ET scheme. To demonstrate the superiority in reducing the communication burden, we compare the following three LFC schemes: 1) the ET LFC scheme is proposed in Wen et al. [15]; 2) the AET LFC scheme is introduced in Peng et al. [21]; and 3) the CPSO-ET LFC scheme is proposed in this paper. Moreover, we test the cases with the time-triggered (TT) LFC scheme and without the LFC scheme.

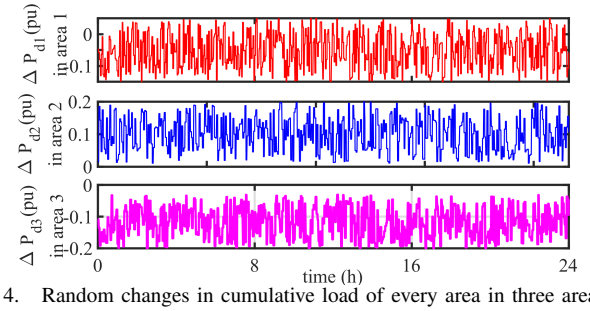

Fig. 4. Random changes in cumulative load of every area in three areas.

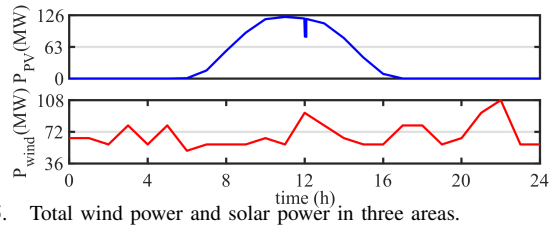

Fig. 5. Total wind power and solar power in three areas.

C. Simulation and Evaluation

Under $\bar{\delta} = 3$, $h = 4s$, $\alpha = 0.1$ and $\tau_M = 1s$, the system is tested with random load disturbances and intermittent fluctuations of wind power and solar power within one day. The random changes in cumulative load of every area are shown in Fig. 4, and the intermittent fluctuations of wind power and solar power are plotted in Fig. 5.

The frequency deviation and control input for generator 1 (G1), the threshold parameters and the transmission instant of area 1 are shown in Figs. 6-9, respectively. The responses in areas 2 and 3 are similar and omitted. The transmission amount of measurement/control signals (TAMC) of every area for different LFC schemes are shown in Table II. For comparison, the TAMC of the TT LFC scheme are listed in Table II. Moreover, the values of $(CF_i)_1$ in CPS1 definition within one day are shown in Fig. 10, and the numbers of $|(ACE_i)_{10min}| \leq L_{10-i}$ (NAL) in CPS2 definition within one day are displayed in Table II.

TABLE II
TAMC AND NAL FOR CPS2 WITHIN ONE DAY IN DIFFERENT SCHEMES

	CPSO-ET		AET		ET		TT		no LFC
	TAMC	NAL	TAMC	NAL	TAMC	NAL	TAMC	NAL	NAL
Area 1	916	144	2580	144	3031	144	21600	144	10
Area 2	4842	144	8599	144	9534	144	21600	144	10
Area 3	2494	144	4911	144	5718	144	21600	144	10

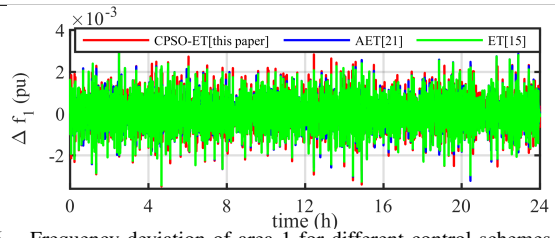

Fig. 6. Frequency deviation of area 1 for different control schemes.

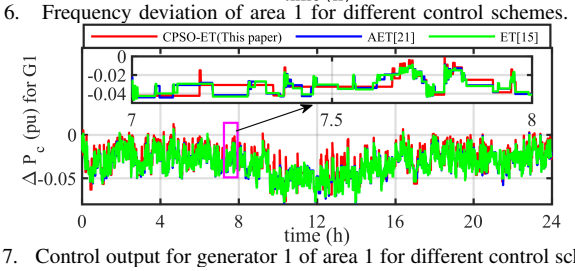

Fig. 7. Control output for generator 1 of area 1 for different control schemes.

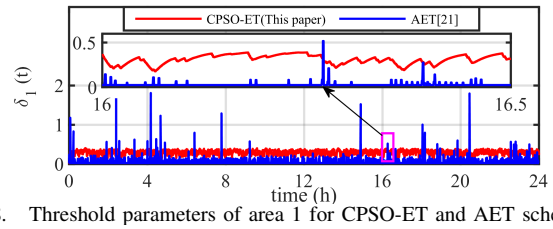

Fig. 8. Threshold parameters of area 1 for CPSO-ET and AET schemes.

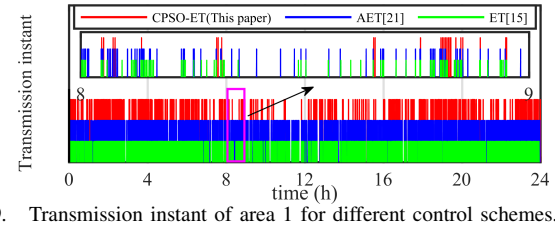

Fig. 9. Transmission instant of area 1 for different control schemes.

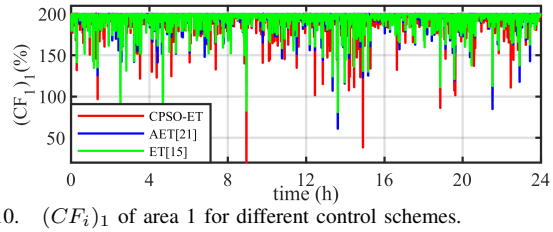

Fig. 10. $(CF_i)_1$ of area 1 for different control schemes.

As presented by Fig. 8, the proposed scheme obtains larger threshold parameters of the ET scheme at most sampling instants to lower the triggering frequency. Additionally, the proposed scheme effectively adjusts the threshold parameters and maintains a stable value, while the threshold parameters in the AET LFC scheme change dramatically. In Figs. 7 and 9 and Table II, the proposed scheme significantly reduces the unnecessary amounts of measurement/control signals transmission. Specifically, the TAMC of areas 1, 2, and 3 are

reduced by 64.50%, 43.69%, and 49.22%, respectively, compared with those in the AET scheme. The frequency deviation in the proposed scheme is slightly larger than those in the AET and ET schemes from Fig. 6. The values of $(CF_i)_1$ in the proposed scheme are similar to those in the AET and ET schemes from Fig. 10. By making a simple calculation, the average value of $(CF_i)_1$ during one day is 191.73% and satisfies the requirement of CPS1. Additionally, the NAL in the proposed scheme are 144 and same as those obtained by the AET and ET schemes for every area from Table II. This meets the requirement introduced in (16) in CPS2. These results demonstrate the effectiveness of the proposed scheme.

D. Discussion

1) The use of the proposed scheme will be accompanied by sacrificing more system dynamic performance than the existing schemes. This results in performance degradation over some short periods, i.e., the values of $(CF_i)_1$ below 100%, as shown in Fig. 10. Based on the CPSO-ET scheme, the occurrence of performance degradation can drive the threshold parameter to decrease, thereby increasing the triggering frequency. Then it can increase the transmission amount of control signals at a fixed time interval so that the actuator can receive more updated control signals to timely adjust the system state to improve the system control performance and meet the requirements of CPSs.

2) Due to the large difference of the generation and load and the intermittently updating of the control signals based on the ET condition (7), the adjacent control output vary greatly. This will cause a sharp change in control input to the actuator. In the practical LFC scheme, the controller output is generally accompanied by a device with the limitations of both the amplitude and the rate-of-change. It limits the excessive change of the controller output to reduce the impact on the actuator. Like most LFC schemes in [5]–[23], the relevant nonlinear characteristics, including the limitations of the controller output and the inherent physical constraint of generation rate, are not considered in the design of the proposed control scheme, since the LFC itself is a slow regulation process and considering these nonlinear characteristics in the controller design is complex. Then, to valid the effectiveness of the proposed control scheme, these nonlinear constraints are added in the simulation tests. Moreover, the proposed scheme shows advantages in coping with performance degradation caused by these constraints in comparison with the existing schemes, since it can maintain the requirements of CPS1 and CPS2 under the action of the CPSO parameter regulation. A certain degree of performance degradation caused by these nonlinear constraints will not affect the feasibility of the proposed scheme.

*3)*To better or completely overcome the effects of the nonlinear characteristics, Baiomy et al. [35] presented effective control methods for linear systems by considering directly the amplitude- and rate-saturated characteristic in the controller design. Based on the methods in [35], the proposed scheme in this paper can be improved by considering directly the nonlinearities of the controller output and the generation rate constraint in the controller design, and will be our future research work. Moreover, some power systems require wind power generators to participate in the frequency regulation [36]. How to modify the proposed scheme with the frequency regulation support provided by the wind power generators is an interesting research direction.

V. Conclusions

In this paper, a decentralized CPSO-ET LFC scheme has been proposed for multi-area power systems under limited communication bandwidth. The proposed scheme effectively reduces the usage of communication network bandwidth, while ensuring that the frequency and tie-line power of power systems satisfy CPS1 and CPS2 of NERC. In addition, the use of decentralized control strategy ensures the scalability of the proposed scheme in large-scale interconnected power systems. The effectiveness of the proposed scheme has been validated based on the IEEE 39-bus system simulation test.

Appendix A
Proof for Theorem 1

Choose a Lyapunov-Krasovskii functional as follows

$$V(x_i(t)) = V_1(t) + V_2(t) \tag{21}$$

where

$$V_1(t) = \xi_1{}^T P_1 \xi_1 + \int_{t-\tau_M}^{t} \xi_2{}^T P_2 \xi_2 ds + \int_{-\tau_M}^{0}\int_{t+\theta}^{t} \dot{x}_i^T(s) P_3 \dot{x}_i(s) d\theta ds$$

$$V_2(t) = h_{d(t)} \xi_3{}^T X \xi_3 + h_{d(t)} \int_{t-\varsigma(t)}^{t-\tau_M} \dot{x}_i^T(s) Z \dot{x}_i(s) ds$$

with $h_{d(t)} = \eta_M - \varsigma(t)$, $\eta_M = h + \tau_M$, $\xi_1 = \left[x_i{}^T(t)\ x_i{}^T(t-\tau_M)\right]^T$, $\xi_2 = \left[x_i^T(s)\ \dot{x}_i^T(s)\right]^T$, and $\xi_3 = \left[x_i^T(t-\tau_M)\ x_i^T(t-\varsigma(t))\right]^T$. The matrices P_i with $i = 1, 2, 3$, X and Z are defined as Theorem 1 without superscript $\hat{}$.

For system (10) with $\omega_i(t) = 0$, any matrix L satisfies the following zero-equation based on the free-weight-matrix technique:

$$0 = 2\xi_4^T L \left(\dot{x}_i(t) - A_i x_i(t) - B_i K_i C_i (e(i_j h) - x_i(t-\varsigma(t)))\right) \tag{22}$$

Based on Newton-Leibnitz formula, one can obtain $\int_{t-\varsigma(t)}^{t-\tau_M} \dot{x}_i(s) ds = x_i(t-\tau_M) - x_i(t-\varsigma(t))$. Similarly, any matrix M satisfies the following zero-equation based on the free-weight-matrix technique,

$$0 = 2\xi^T M \left(x_i(t-\tau_M) - x_i(t-\varsigma(t)) - \int_{t-\varsigma(t)}^{t-\tau_M} \dot{x}_i(s) ds \right) \tag{23}$$

where $\xi_4 = [x_i^T(t),\ x_i^T(t-\varsigma(t)),\ \dot{x}_i^T(t)]^T$ and $\xi = [x_i^T(t),\ x_i^T(t-\varsigma(t)),\ x_i^T(t-\tau_M),\ \dot{x}_i^T(t-\tau_M),\ \dot{x}_i^T(t),\ e(i_j h)^T]^T$. Then, calculating the derivative of $V(x_i(t))$ along the trajectory of system (10), one can obtain

$$\begin{aligned}\dot{V}_1(x_i(t)) =& 2\xi_1^T P_1 \xi_1 + \tau_M \dot{x}_i^T(t) P_3 \dot{x}_i(t) - \int_{t-\tau_M}^{t} \dot{x}_i^T(s) P_3 \dot{x}_i(s) ds \\ &+ \begin{bmatrix} x_i(t) \\ \dot{x}_i(t) \end{bmatrix}^T P_2 \begin{bmatrix} x_i(t) \\ \dot{x}_i(t) \end{bmatrix} - \begin{bmatrix} x_i(t-\tau_M) \\ \dot{x}_i(t-\tau_M) \end{bmatrix}^T P_2 \begin{bmatrix} x_i(t-\tau_M) \\ \dot{x}_i(t-\tau_M) \end{bmatrix} \\ \dot{V}_2(x_i(t)) =& -\xi_3^T X \xi_3 - \int_{t-\varsigma(t)}^{t-\tau_M} \dot{x}_i^T(s) Z \dot{x}_i(s) ds \\ &+ h_{d(t)} (2\xi_3^T X \dot{\xi}_3 + \dot{x}_i^T(t-\tau_M) Z \dot{x}_i(t-\tau_M))\end{aligned}$$

Next, use Jensen inequality to estimate integral items of P_3

$$\begin{aligned}&-\int_{t-\tau_M}^{t} \dot{x}_i^T(s) P_3 \dot{x}_i(s) ds \\ &\qquad \le -\frac{1}{\tau_M} (x_i(t) - x_i(t-\tau_M))^T P_3 (x_i(t) - x_i(t-\tau_M))\end{aligned}$$

and add zero-equations (22) and (23) and the ET condition (7) into the derivative. This yields

$$\dot{V}(x_i(t)) = \frac{h_{d(t)}}{h} \xi^T \Xi_1 \xi + \frac{1}{h} \int_{t-\varsigma(t)}^{t-\tau_M} \begin{bmatrix} \xi \\ \dot{x}_i(s) \end{bmatrix}^T \Xi_2 \begin{bmatrix} \xi \\ \dot{x}_i(s) \end{bmatrix} ds \tag{24}$$

where

$$\Xi_1 = \psi_1 + \Gamma + h\psi_2 \tag{25}$$

$$\Xi_2 = \begin{bmatrix} \psi_1 + \Gamma & -h\Upsilon_2^T M \\ * & -hZ \end{bmatrix} \tag{26}$$

with $\Gamma = Sym\{\Upsilon_1^T L(e_5 - A_i e_1 - B_i K_i C_i (e_6 - e_2))\}$; the other parameters are given in Theorem 1 without superscript $\hat{}$. It should be noted that $V_2(t)$ is a looped functional, and $V_2(t-\varsigma(t)) = 0$ for $k = 0, 1, 2, \ldots$. If $\Xi_1 < 0$

and $\Xi_2 < 0$ hold, $\dot{V}(x_i(t)) < 0$. System (10) is then asymptotically stable according to Theorem 1 in [32].

Next, define $\hat{x}_i(t) = e^{\lambda t}x_i(t)$. Since $e^{\lambda\varsigma(t)} \in [\rho_1, \rho_2]$, system (10) can be represented in the following polytopic form:

$$\dot{\hat{x}}_i(t)=\sum_{j=1}^{2}\mu_j(t)\{(A_i+\lambda I)\hat{x}_i(t)+\rho_j B_i K_i C_i(\hat{e}(i_j h)-\hat{x}_i(t-\varsigma(t)))\} \quad (27)$$

where $\hat{e}(i_j h) = \hat{x}_i(i_j h) - \hat{x}_i(t_k h)$, $\mu_1(t) = (\rho_2 - e^{\lambda\varsigma(t)})/(\rho_2 - \rho_1)$ and $\mu_2(t) = (e^{\lambda\varsigma(t)} - \rho_1)/(\rho_2 - \rho_1)$. Note that the LMIs $\Xi_1 <0$ and $\Xi_2 <0$ are affine in the system matrices. Therefore, to guarantee asymptotic stability of system (27), we have to simultaneously solve LMIs $\Xi_1 <0$ and $\Xi_2 <0$ for the two vertices of system (27) given by $\rho_1 B_i K_i C_i$ and $\rho_2 B_i K_i C_i$, where the same decision matrices are applied.

Then, updating the system matrices of LMIs $\Xi_1 <0$ and $\Xi_2 <0$ with system (27) in the two vertices of $\rho_1 B_i K_i C_i$ and $\rho_2 B_i K_i C_i$, we can obtain

$$\Xi_{1f} =\psi_1 + \Gamma_f + h\psi_2 < 0 \quad (28)$$

$$\Xi_{2f} = \begin{bmatrix} \psi_1 + \Gamma_f & -h\Upsilon_2^T M \\ * & -h\hat{Z} \end{bmatrix} < 0 \quad (29)$$

with $f = 1, 2, \Gamma_f = Sym\{\Upsilon_1^T L(e_5-(A_i+\lambda I)e_1-\rho_f B_i K_i C_i(e_6-e_2))\}$ and the other parameters given in Theorem 1 without superscript $\hat{}$. Based on the above proof process and the polytopic characteristic, if LMIs $\Xi_{1f} < 0$ and $\Xi_{2f} < 0$ hold, system (27) is asymptotically stable. In this case, following the exponential stability analysis method for the sampled-data system in [33], system (10) is exponentially stable.

Finally, define $L = [S; aS; bS]$ with tuning parameters a and b, $\hat{S} = S^{-1}$, $\hat{P}_3 = \hat{S}P_3\hat{S}^T$,$\hat{\Omega} = \hat{S}\Omega\hat{S}^T$,$\hat{Z} = \hat{S}Z\hat{S}^T$; $\hat{P}_1, \hat{P}_2$ and $\hat{X}_i$ are defined by pre- and post-multiplying both sides of P_1, P_2 and X_i with $diag\{\hat{S}, \hat{S}\}$ and its transpose, respectively; $\hat{M} = diag\{\hat{S}, \hat{S}, \hat{S}, \hat{S}, \hat{S}, \hat{S}\}M\hat{S}^T$; pre- and post-multiplying (25) by $diag\{\hat{S}, \hat{S}, \hat{S}, \hat{S}, \hat{S}, \hat{S}\}$ and its transpose, respectively; and pre- and post-multiplying (26) by $diag\{\hat{S}, \hat{S}, \hat{S}, \hat{S}, \hat{S}, \hat{S}, \hat{S}\}$ and its transpose, respectively. To develop the controller gains, we define $Y = B_i K_i C_i \hat{S}^T$ to transform the non-LMIs form into the LMIs form. One can obtain $\hat{\Xi}_{1f}$ and $\hat{\Xi}_{2f}$. Then if $\hat{\Xi}_{1f} < 0$ and $\hat{\Xi}_{2f} < 0$ hold, system (10) is exponentially stable with an EDR λ. Moreover, the gains of the PI controller can be calculated by $K_i = Y(\hat{S}^T)^{-1}C_i^T(C_i C_i^T)^{-1}$. This completes the proof.

REFERENCES

[1] H. Bevrani. *Robust Power System Frequency Control*. New York: Springer, 2014.

[2] H. Chen, R. Ye, X. Wang, et al. "Cooperative control of power system load and frequency by using differential games", *IEEE Trans. Control Syst. Technol.*, vol. 23, no. 3, pp. 882–897, May 2015.

[3] H. Shayeghi, A. Jalili, H. A. Shayanfar. "Robust modified GA based multi-stage fuzzy LFC", *Energ. Convers. Manage.*, vol. 48, no. 5, pp. 1656–1670, May 2007.

[4] A. Pappachen, A. P. Fathima. "Critical research areas on load frequency control issues in a deregulated power system: A state-of-the-art-of-review", *Renewable Sustainable Energy Rev.*, vol. 72, pp. 163–177, May 2017.

[5] X. Yu, K. Tomsovic. "Application of linear matrix inequalities for load frequency control with communication delays", *IEEE Trans. Power Syst.*, vol. 19, no. 3, pp. 1508–1515, 2004.

[6] L. Jiang, W. Yao, Q. H. Wu, et al. "Delay-dependent stability for load frequency control with constant and time-varying delays", *IEEE Trans. Power Syst.*, vol. 27, no. 2, pp. 932–941, May 2012.

[7] L. Jin, C. K. Zhang, Y. He, et al. "Delay-dependent stability analysis of multi-area load frequency control with enhanced accuracy and computation efficiency", *IEEE Trans. Power Syst.*, vol. 34, no. 5, pp. 3687–3696, Sept. 2019.

[8] L. Jin, Y. He, C. K. Zhang, et al. "Robust delay-dependent load frequency control of wind power system based on a novel reconstructed model", *IEEE Trans. Cybern.*, 2021. Doi: 10.1109/TCYB.2021.3051160.

[9] C. K. Zhang, L. Jiang, Q. H. Wu, et al. "Delay-dependent robust load frequency control for time delay power systems", *IEEE Trans. Power Syst.*, vol. 28, no. 4, pp. 2192–2201, Aug. 2013.

[10] S. Trip, M. Cucuzzella, C. De Persis, et al., "Passivity-based design of sliding modes for optimal load frequency control", *IEEE Trans. Control Syst. Technol.*, vol. 27, no. 5, pp. 1893–1906, Sept. 2019.

[11] H. Luo, I. A. Hiskens, Z. Hu. "Stability analysis of load frequency control systems with sampling and transmission delay", *IEEE Trans. Power Syst.*, vol. 35, no. 5, pp. 3603–3615, Sept. 2020.

[12] X. C. Shangguan, C. K. Zhang, Y. He, et al. "Robust load frequency control for power system considering transmission delay and sampling period", *IEEE Trans. Ind. Inf.*, 2020. Doi: 10.1109/TII.2020.3026336.

[13] X. C. Shangguan, Y. He, C. K. Zhang, et al. "Switching system-based load frequency control for multi-area power system resilient to denial-of-service attacks", *Control Eng. Pract.*, vol. 107, pp. 104678, Feb. 2021.

[14] Y. Wang, I. R. Pordanjani, W. Xu. "An event-driven demand response scheme for power system security enhancement", *IEEE Trans. Smart Grid*, vol. 2, no. 1, pp. 23–29, March 2011.

[15] S. Wen, X. Yu, Z. Zeng, et al. "Event-triggering load frequency control for multi-area power systems with communication delays", *IEEE Trans. Ind. Electron.*, vol. 63, no. 2, pp. 1308–1317, Feb. 2016.

[16] P. Dahiya, P. Mukhija, A. R. Saxena. "Design of sampled data and event-triggered load frequency controller for isolated hybrid power system", *Int. J. Electr. Power Energ. Syst.*, vol. 100, pp. 331–349, Sept. 2018.

[17] X. C. Shangguan, Y. He, C. K. Zhang, et al. "Sampled-data based discrete and fast load frequency control for power systems with wind power", *Appl. Energ.*,vol. 259, no. 114202, Feb. 2020.

[18] X. Su, X. Liu, Y. D. Song. "Event-triggered sliding-mode control for multi-area power systems", *IEEE Trans. Ind. Electron.*, vol. 64, no. 8, pp. 6732–6741, Aug. 2017.

[19] L. Dong, Y. Tang, H. He, et al. "An event-triggered approach for load frequency control with supplementary ADP", *IEEE Trans. Power Syst.*, vol. 32, no. 1, pp. 581–589, Jan. 2017.

[20] S. Liu, W. Luo, L. Wu. "Co-design of distributed model-based control and event-triggering scheme for load frequency regulation in smart grids", *IEEE Trans. Syst. Man Cybern. Syst.*, vol. 50, no. 9, pp. 3311–3319, Sept. 2020.

[21] C. Peng, J. Zhang, H. Yan. "Adaptive event-triggering H_∞ load frequency control for network-based power systems", *IEEE Trans. Ind. Electron.*, vol. 65, no. 2, pp. 1685–1694, Feb. 2018.

[22] H. Li, X. Wang, J. Xiao. "Adaptive event-triggered load frequency control for interconnected microgrids by observer-based sliding mode control", *IEEE Access*, vol. 7, pp. 68271–68280, May 2019.

[23] H. Zhang, S. Su, Y.Y. Zhao, et al. "Networked load frequency control of multi-area uncertain power systems via adaptive event-triggered communication scheme", *J. Franklin Inst.*, vol. 356, no. 16, pp. 9600–9626, Nov. 2019.

[24] M. Yao, R. R. Shoults, R. Kelm. "AGC logic based on NERC's new control performance standard and disturbance control standard", *IEEE Trans. Power Syst.*, vol. 15, no. 2, pp. 852–857, May 2000.

[25] A. Feliachi, D. Rerkpreedapong. "NERC compliant load frequency control design using fuzzy rules", *Electr. Power Syst. Res.*, vol. 73, no. 2, pp.101–106, Feb. 2005.

[26] D. Rerkpreedapong, A. Feliachi. "Fuzzy rule based load frequency control in compliance with NERC's standards", *IEEE Power Eng. Soc. Summer Meeting*, IEEE, vol. 3, pp. 1154–1159, July 2002.

[27] A. Pappachen, A. P. Fathima. "NERCs control performance standards based load frequency controller for a multi area deregulated power system with ANFIS approach", *Ain Shams Eng. J.* , vol. 9, no. 4, pp.2399–2414, Dec. 2018.

[28] S. K. Pandey, S. R. Mohanty, N. Kishor. "A literature survey on load-frequency control for conventional and distribution generation power systems", *Renewable Sustainable Energy Rev.*, vol. 25, pp. 318–334, Sept. 2013.

[29] Y. Mi, Y. Fu, C. Wang, P. Wang. "Decentralized sliding mode load frequency control for multi-area power systems", *IEEE Trans. Power Syst.*, vol. 28, no. 4, pp. 4301–4309, Nov. 2013.

[30] D. Yue, E. Tian, Q. Han. "A delay system method for designing event-triggered controllers of networked control systems", *IEEE Trans. Autom. Control*, vol. 58, no. 2, pp. 475–481, Feb. 2013.

[31] C. Peng, T. C. Yang. "Event-triggered communication and H_∞ control co-design for networked control systems", *Automatica*, vol. 49, no. 5, pp. 1326–1332, May 2013.

[32] A. Seuret. "A novel stability analysis of linear systems under asynchronous samplings", *Automatica*, vol. 48, no. 1, pp. 177–182, Jan. 2012.

[33] K. Liu, E. Fridman. "Wirtinger's inequality and Lyapunov-based sampled-data stabilization", *Automatica*, vol. 48, no. 1, pp. 102–108, Jan. 2012.

[34] I. Hiskens. "IEEE PES task force on benchmark systems for stability controls", *Tech. Rep. 39-bus system*, 2013.

[35] N. Baiomy, R. Kikuuwe. "An amplitude- and rate-saturated controller for linear plants", *Asian J. Control*, vol. 22, no. 1, pp. 77–91, Jan. 2020.

[36] X. Peng, W. Yao, C. Yan. "Two-stage variable proportion coefficient based frequency support of grid-connected DFIG-WTs", *IEEE Trans. Power Syst.*, vol. 35, no. 2, pp. 962-974, March 2020.